REVIEW

DOI: 10.1002/cjoc.201500755

Lanthanide-Doped Nanoparticles with Near-Infrared-to-Near-Infrared Luminescence for Bioimaging

Yurong Wei,[a,b] Xiangdong Yang,[b] Yurou Ma,[b] Shengfu Wang,*[,a] and Quan Yuan*[,b]

[a] *Ministry of Education, Key Laboratory for the Synthesis and Application of Organic Functional Molecules & College of Chemistry and Chemical Engineering, Hubei University, Wuhan, Hubei 430062, China*
[b] *Key Laboratory of Analytical Chemistry for Biology and Medicine (Ministry of Education), College of Chemistry and Molecular Sciences, Wuhan University, Wuhan, Hubei 430072, China*

Lanthanide (Ln, or rare-earth) doped nanoparticles are well-known for their prominent optical properties and have been widely used for biological applications, especially in biological assays and medical imaging. Recently, the extensive attention of near infrared (NIR) wavelength range has dramatically increased for its fast feedback, high spatial resolution and deep tissue penetration. Tissues have minimal absorbance in this region. While a lot of excellent reviews cover various aspects of biomedical imaging based on lanthanide doped nanoparticles, there has not been a review that systematically summarizes NIR-to-NIR imaging with lanthanide doped nanoparticles. In this review, we focus on the recent development of NIR-to-NIR imaging based on lanthanide doped nanoparticles, and discuss challenges and opportunities in it.

Keywords lanthanide, up-conversion, down-converion, near-infrared, bioimaging

Introduction

In the past few decades, bioimaging has been widely studied in biomedical sciences for applications from non-invasive monitor of the cellular functions to real-time observation of biological processes in complicated living system, which significantly promoted the developments of early stage diseases diagnosis and early intervention therapy. Among all of the imaging strategies, luminescent bioimaging is regarded as one of the most promising imaging techniques for its numerous superior properties, such as high sensitivity, good resolution and fast feedback. Despite all that advantages, there are still sorts of challenges confronted by luminescent bioimaging, such as limitation of penetration depth of emission light and autofluorescence interference.[1] To be specific, the emission peaks of traditional fluorophores usually lie in the visible region ranging from 400 to 650 nm. It is well known that water and biological tissues such as skin and blood can significantly absorb or scatter the visible light (Figure 1),[2] which leads to the attenuation of light emitted by the traditional fluorophores.[3] Moreover, such attenuation effect is proportional to the depth of the target tissue and visible light usually gives tissue penetration depth of only about 1 mm,[4] suggesting the weakness of traditional fluorophores in deep tissue imaging. Also, the traditional fluorophores are usually excited by ultraviolet and visible light, which inevitably activates the fluorophores in biological tissues and leads to the so-called autofluorescence. Such autofluorescence may significantly decrease the sensitivity and resolution of luminescent bioimaging. In addition, the short wavelength incident light can also cause potential photodamage to the illuminated tissues. Thus, developing novel luminescent agents that can simultaneously avoid the absorption/scattering caused by biological tissues and eliminate autofluorescence interference is highly desired for luminescent bioimaging.

In order to obtain deeper tissue penetration, more efforts have been made in the exploitation of imaging agents with emissions locating in the "biological transparency window". The "biological transparency window" refers to two near-infrared (NIR) regions (I: 650—900 nm, II: 1000—1450 nm) in which water and biological tissues show minimal absorption.[5] Moreover, long wavelength NIR light suffers less from scattering effect than short wavelength visible light, further suggesting the potential of NIR emitting agents for deep tissue imaging. Since 1990s, NIR I bioimaging has attracted significant attention in bionanotechnology and biomedical fields. The first study about *in vivo* imaging of tumors with NIR emitting agents was reported by Weissleder and co-workers[6] in 1999. They made use of a protease-activated near-infrared fluorescent probe for tumor imaging in a xenograft mouse model and obtained desired images at high resolution. In NIR I biomedical

* E-mail: yuanquan@whu.edu.cn
Received October 30, 2015; accepted December 10, 2015; published online February 3, 2016.

CHINESE JOURNAL OF CHEMISTRY

imaging window, the tissue penetration depth can be up to 1—2 cm in practice, much deeper than that of traditional visible light.[7] In 2003, Lim and co-workers conducted systematic simulations and modeling studies of bioimaging with NIR quantum dots (1320 nm), and they summarized that the signal-to-noise ratios of bioimaging could be significantly improved by over 100-fold even in turbid media like tissue or blood.[8] Since then, extensive researches have been launched to search for new biocompatible fluorescent probes with emission maximum falling in the "biological transparency window" and encouraging achievements have been made. As for elimination of autofluorescence, developing imaging agent with excitation wavelength locating in the NIR regain has also been demonstrated to be one of the most promising strategies because NIR light cannot activate the fluorophores in biological tissues and thus will not cause any autofluorescence.[9-18] Here we can safely come to the conclusion that developing imaging agents with both the excitation and emission lights locating in the "optical transmission window" of biological tissues (designated as NIR-to-NIR luminescence) is the ideal approach to improve the sensitivity and resolution of luminescent bioimaging.

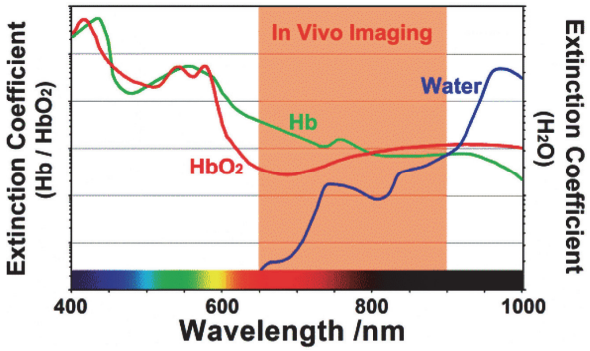

Figure 1 Optical NIR I windows in biological tissues and water (Hb: hemoglobin; HbO_2: oxyhemoglobin). Reproduced with permission.[2] Copyright 2013, WILEY-VCH Verlag GmbH & Co. KGaA, Weinhei.

Till now, several materials with NIR-to-NIR luminescence have been reported, such as infrared quantum dots (QDs), single-walled carbon nanotubes (SWCNTs) and lanthanide-doped nanomaterials. Even though infrared QDs possess advantages such as high quantum yields (QYs) and good photostability, their applications in luminescent bioimaging are largely blocked by their inner toxic elements, for instance, lead and arsenic. Ag_2S QDs is a rare kind of QDs that features low toxicity, but it suffers from serious quenching effect caused by air or irradiation.[1] SWCNTs have drawn much attention in bioimaging in the past few years and many studies have demonstrated their ability to achieve deep tissue penetration and high sensitivity in *in vivo* imaging of blood vessels beneath or in deep layers of skin. However, there are several drawbacks founded associated with SWCNTs that cannot be ignored before their widespread application. For example, their broad length distributions span hundreds of nanometers.[19] Besides, the needle-like structures may cause chronic toxicity and tissue damage, which have already been observed in lungs of mice after SWCNTs inhalation.[20] Compared with infrared QDs and SWCNTs, lanthanide ions (Ln^{3+})-doped nanoparticles have aroused significant interest recently and show great promise for serving as a new class of NIR-to-NIR fluorophores for future deep-tissue bioimaging.[21,22] Lanthanide elements are species with abundant f-orbital configurations and it is their unique electronic structure that enables Ln^{3+} ions in solids to give rise to a rich energy level from ultraviolet to visible or infrared, suggesting efficient NIR-to-NIR luminescence can be generated through doping Ln^{3+} ions into suitable matrices. Moreover, since the energy levels of Ln^{3+} are well-defined due to the effective shielding of the 4f orbitals by the outer-lying filled 5s and 5p orbitals, lanthanide-doped nanoparticles can efficiently minimize the effect of the outer ligand fields. Furthermore, the spectra arising from inner-shell 4f-4f transitions are narrow and insensitive to outer environment. All of the above features endow lanthanide-doped nanoparticles with tunable and sharp emissions as well as exceptional photostability.[23,24] Lanthanide-doped nanoparticles typically have distinct emission line widths of about 10—20 nm (full width at half maximum), which is much narrower than that of quantum dots (*ca.* 25—40 nm) or transition metal ions (*ca.* 100 nm).[25] What's more, since lanthanide emissions involve only atomic transitions, they are extremely resistant to photobleaching. Such attractive characteristics make lanthanide doped NIR-to-NIR nanoparticles promising as bioimaging probes.[26]

Scheme 1 Bioimaging applications of lanthanide doped nanoparticles with NIR-to-NIR luminescence

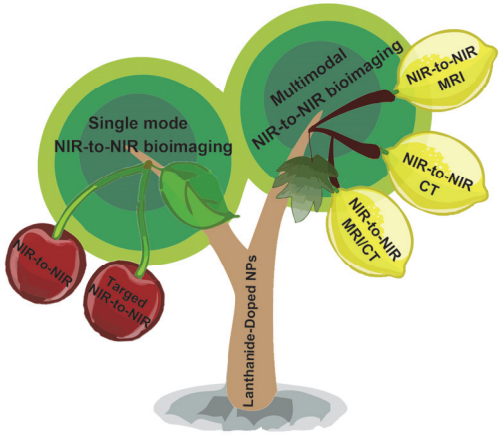

In this review, we focus on the recent bioimaging development of lanthanide-doped nanoparticles that can be excited by NIR light and further emit in NIR I or NIR II regions. Firstly, basic concepts and theories on NIR-to-NIR luminescence will be introduced. Secondly,

the effective methods to enhance the intensity of NIR-to-NIR luminescence are discussed. Finally, the recent research progress on bioimaging applications of lanthanide-doped nanoparticles will be highlighted, including the instrumentation, single mode NIR-to-NIR bioimaging and multimodal NIR-to-NIR bioimaging.

NIR-to-NIR Luminescent Properties of Lanthanide-doped Nanomaterials

Based on the specific mechanism, luminescence can be divided into two categories: up-conversion (UC) and down-conversion (DC) emission. Up-conversion luminescence (UCL) is a non-linear, anti-Stokes process, in which two or more lower energy excitation photons are converted to higher energy photons on the basis of sequential adsorption and energy transfer steps. While the DC process obeys Stokes' law, which refers to the conversion of higher energy photons into lower energy photons. Such two processes can occur simultaneously in a single nanoparticle. According to the mechanism of luminescence, lanthanide-doped NIR-to-NIR luminescent nanoparticles can be divided into three categories: NIR-to-NIR UC nanoparticles, NIR-to-NIR DC nanoparticles, and dual-modal NIR-to-NIR luminescent nanoparticles. NIR-to-NIR UC and DC nanoparticles usually can be differentiated by the sorts of doped Ln^{3+} ions. While dual-modal NIR-to-NIR luminescence nanoparticles may be doped with both the Ln^{3+} ions with NIR-to-NIR UC and DC luminescence. It should be noted that the similar chemical properties were also found in all the lanthanides when doping with the same emissive Ln^{3+} ion, and in general, the crystal structure of Ln^{3+}-doped material keeps the same as that of the undoped matrix. Table 1 summarizes representative works on lanthanide-doped nanoparticles with NIR-to-NIR luminescence. In this part, we will introduce the basic conceptions for Ln^{3+}-doped nanoparticles with NIR-to-NIR luminescence and present an overview of the dopant/host design principle for efficient NIR-to-NIR luminescence.

NIR-to-NIR UC luminescence

As we mentioned above, UC materials are able to convert lower-energy near-infrared photons to higher-energy ones.[27] Efficient UC process usually consists of three components: a host matrix, a sensitizer and an activator. In order to obtain efficient NIR-to-NIR UCL, the selection of these three components should obey strict criteria. Ideal host materials are required to be optically transparent and possess low lattice phonon energy to guarantee minimized nonradiative losses and maximized radiative emission. Currently, $NaYF_4$,[28] $NaGdF_4$,[29] $NaLuF_4$,[30] LaF_3,[31] CaF_2[32] *etc.* have been widely employed as host materials for the NIR-to-NIR UCL. Among them, fluorides have been regarded as the most efficient host materials due to their low phonon energies (*ca.* 350 cm^{-1}) and high chemical stability. Sensitizers need to have cross-section in the NIR region, and they are also co-doped with activator to form efficient energy transfer up-conversion (ETU) process between sensitizer and activator. Among all reported sensitizers, Yb^{3+} displays an extremely simple energy level with only one excited 4f level ($^2F_{5/2}$). For these reasons, Yb^{3+} has a larger absorption cross-section around 980 nm than that of any other lanthanide ions due to its $^2F_{7/2}\rightarrow{}^2F_{5/2}$ transition. Therefore, Yb^{3+} is currently the most efficient sensitizer to yield strong NIR UCL. Prasad[33] presented a simple method to increase NIR-to-NIR UCL intensity by simply replacing of Y^{3+} ions with Yb^{3+} ions in the nanocrystal. The NIR-to-NIR UCL intensity of the $NaYbF_4$:2% Tm^{3+} nanoparticles was demonstrated to be 4 times that of $NaYF_4$:20% Yb^{3+}/2% Tm^{3+} nanoparticles. Finally, the rational selection of proper lanthanide ions as the activator is also very important for efficient NIR-NIR UCL. The lanthanide ions Er^{3+}, Tm^{3+} and Ho^{3+}, which possess ladder-like arranged energy levels, are usually co-doped with Yb^{3+} and serve as activators to enhance the NIR UCL efficiency under NIR excitation. Among the above activators, Tm^{3+} ions are the most frequently employed because they show strong NIR emission from 750 to 850 nm due to the $^3H_4$-$^3H_6$ transition. Furthermore, the transition is well resonant with that of Yb^{3+}, which facilitated the efficient energy transfer from Yb^{3+} to Tm^{3+} ions. Therefore, Yb^{3+} and Tm^{3+} couple have been widely adopted to prepare NIR-to-NIR UC nanomaterials with emissions at around 800 upon excitation of the 980 nm laser diodes. Li and co-workers have co-doped Yb^{3+} sensitizer and Tm^{3+} activator into different host matrixes such as $NaGdF_4$,[29] $NaYF_4$,[28] $NaLuF_4$[30] to study their NIR-to-NIR UCL performance. Additionally, CaF_3,[34] $CaMoO_4$,[35] $KGdF_4$[36] and Y_2O_3[37] have also been reported to produce strong NIR-to-NIR UCL upon excitation at 980 nm when doped with Tm^{3+} and Yb^{3+} ions. Even though efficient NIR-to-NIR UCL has been achieved, it is still worth pointing out that excitation at around 980 nm suffers from some intrinsic disadvantages, such as limited tissues penetration depth and unavoidable heat generation. The water molecules in biological tissues would strongly absorb the incident light (980 nm) and overwhelmingly attenuate its intensity, which significantly decrease the penetration depth of the incident 980 nm light. Furthermore, nearly all of the light energy absorbed by biological samples would be transformed into local heating energy, which could probably induce heat damage in cells and tissues. To alleviate this problem, Andersson-Engels and co-workers proposed a promising alternative strategy by exciting the UC NIR phosphors ($NaYbF_4$:Yb^{3+}/Er^{3+}, Yb^{3+}/Ho^{3+}, Yb^{3+}/Tm^{3+}) at around 915 nm and they observed even more efficient NIR-to-NIR UCL.[38] They also verified that this novel laser excitation wavelength allowed drastically less heating of the biological specimen and provided larger imaging depth in the animals or tissues due to the mini-

Table 1 Typical examples of lanthanide-doped nanoparticles with NIR-to-NIR luminescence

Lanthanide-doped nanoparticle	Ex/nm	Em/nm	Size/nm	Ref.
$NaYbF_4$:2%Tm^{3+}	980	800	sub-20	69
$NaYF_4$:Tm^{3+},Yb^{3+}	975	800	20－30	59
$NaYF_4$:Yb^{3+}/Tm^{3+}	980	800	7－10	33
$NaYF_4$:20%Yb,1.8%Er,0.2%Tm	980	800	14	31
$NaYF_4$:Yb^{3+},Tm^{3+},Co^{2+}	980	800	33.2	66
$NaYbF_4$:Tm^{3+}/$NaGdF_4$	975	800	12	56
(α-$NaYbF_4$:Tm^{3+})/CaF_2	975	800	27	55
$NaYF_4$:Yb^{3+},Tm^{3+}@FexOy	980	800	20	45
$NaGdF_4Tm^{3+}$/Er^{3+}/Yb^{3+}	980	800	25－55	29
$NaGdF_4$:Nd^{3+}@$NaGdF_4$	740	900, 1050, 1330	15	57
$NaGdF_4$:Yb,Er@$NaGdF_4$:Nd,Yb	808	980, 1064, 1532	22.5±1.1	45
β-$NaGdF_4$/Na(Gd,Yb)F_4:Er/$NaYF_4$:Yb/$NaNdF_4$:Yb	800	1525	11.79±0.77	44
$NaGdF_4$:Nd^{3+},Yb^{3+},Tm^{3+}	800	1050	21	62
$NaLuF_4$:20 mol%Yb,2 mol%Er	980	800	sub-20	30
$NaLuF_4$:Gd^{3+}/Yb^{3+}/Tm^{3+}	980	800	－	65
$NaLuF_4$:Yb^{3+},Tm^{3+}@SiO_2-GdDTPA	980	800	30	75
Y_2O_3:Er^{3+}	980	1550	100	40
CaF_2:Tm^{3+},Yb^{3+}	920	800	11±2	32
$CaMoO_4$:Tm^{3+}, Yb^{3+}	980	800	－	35
GdF_3:Yb^{3+},Tm^{3+}	980	807	40 (spherical)	34
GdF_3:Nd^{3+}	808	1064	5	63
$KGdF_4$:Tm^{3+}2%,Yb^{3+}20%/$KGdF_4$	980	803	7－4	36
Ln^{3+}:BaF_2/Ln^{3+}:SrF_2	975/796	802/1504	7	46

mized absorption by water molecules. It can be concluded that deeper tissue penetration and less heating of the biological specimen were realized in NIR UC bioimaging by using an efficient 915 nm laser after detailed and reasonable comparison with traditional 980 nm laser.

NIR-to-NIR DC luminescence

In comparison with NIR-to-NIR UC process, NIR-to-NIR DC emission is preferred for *in vivo* imaging because of its high quantum yields, deep tissue penetration, high contrast and signal-to-noise ratio. DC luminescent materials are also composed of inorganic matrix and Ln^{3+} doping ions.[39] Several kinds of inorganic compounds have been extensively exploited as host materials, such as rare earth oxide, oxysulfide, fluoride, phosphate, and vanadate. Soga[40] reported a NIR-to-NIR bioimaging system based on Er-doped yttrium oxide (Y_2O_3:Er^{3+}) phosphors with NIR emission at 1550 nm under 980 nm excitation. The kinds of Ln^{3+} luminescent centers are important factors that influence the luminescence performance. Some down-convention emitters of Ln^{3+}, such as Eu^{3+}, Tb^{3+}, Dy^{3+}, Sm^{3+} and Nd^{3+} show great promise for luminescent bioimaging due to their intense and long-lived photo-luminescence (PL). Among the above mentioned emitters, the Nd^{3+} ion is considered as an ideal candidate to improve the pumping efficiency of 800 nm laser diode because it possesses intense absorption cross-section around 800 nm.[41,42] In 2013, the 800 nm excitable UCNPs concept was introduced for the first time by Han and co-workers.[2] They found that a small quantity of Nd^{3+} (doping ratio ⩽ 1%) doping in Yb^{3+}/Er^{3+} (Tm^{3+}) co-doped core/shell *β*-$NaYF_4$ UCNPs was essential for sensitizing at 800 nm. The UCNPs they reported showed a more than 20-fold enhancement of emission intensity than the traditional dual-dopants of Yb^{3+}-sensitized system. In the same year, Liu and co-workers have designed a new type of core-shell structured up-conversion nanoparticles through utilizing Nd^{3+} ions as the sensitizers for 800 nm excitation.[43] Inspiringly, Zhang and co-workers[44] have reported novel Nd^{3+} doped DC nanocrystals (NCs) for *in vivo* NIR imaging with excitation at 800 nm. It is noteworthy that the signals under 800 nm excitation can be easily detected even through 1.8 cm of pork tissue, deeper than the penetration depth reported for the same wavelength excited with a 980 nm laser. As we mentioned above, the heating effect of incident light may cause potential photodamage to the illuminated tissues. The effects of 808 nm laser on cell survival and mouse body have been systematically studied by Yan and co-workers.[45] They observed that nearly all of the tested cells were dead under irradiation with 980 nm laser. However, most of the cells survived

under irradiation of the 808 nm laser. For mouse that illuminated with 980 nm laser for 50 s, a notable local heating effect and obvious temperature rise were observed and a burn wound was discernible 1 day later. In contrast, only a slight temperature rise occurred in mouse even after the 808 nm laser irradiation for 5 min. The above results therefore clearly demonstrated that 808 nm is a biocomparable excitation wavelength for luminescent bioimaging.

When excited with infrared light (NIR I window), NIR-to-NIR DCL peaks usually lie in NIR-II window with short-wavelength infrared light (1000—2300 nm). The NIR-II window features lower tissue autofluorescence and 1000-fold reduction in scattering losses than the NIR I window, enabling unprecedented improvements in penetration depth and resolution. Zhang and co-workers have prepared multi-shell nanocrystals with efficient short-wavelength infrared light emission at 1525 nm for *in vivo* DC NIR imaging.[44] They declared that the probe was detectable in tissues at depths of up to 18 mm with a low detection threshold concentration (5 nmol/L for the stomach of nude mice and 100 nmol/L for the stomach of Sprague-Dawley rats).

Dual-modal NIR-to-NIR luminescence

The fact that both of the dual-mode luminescence peaks are in the NIR region is particularly attractive for the direct applications in multiplexed and highly sensitive bioassays. As we mentioned above, the Tm^{3+}/Yb^{3+} couple was widely used to achieve Tm^{3+} NIR (*ca*. 800 nm) UC luminescence under excitation of 980 nm laser through energy transfer (ET) from Yb^{3+} to Tm^{3+}, and Nd^{3+} ion was a good candidate to achieve efficient DC luminescence. Nanoparticles with both UC and DC luminescence can be rationally designed based on features of Ln^{3+} ions. However, it is not easy to simultaneously achieve both UC emission of Tm^{3+} and DC emission of Nd^{3+} via merely tri-doping of $Tm^{3+}/Yb^{3+}/Nd^{3+}$ into a single host, because ET from Tm^{3+} to Nd^{3+} and from Nd^{3+} to Yb^{3+} could result in quenching of both Tm^{3+}

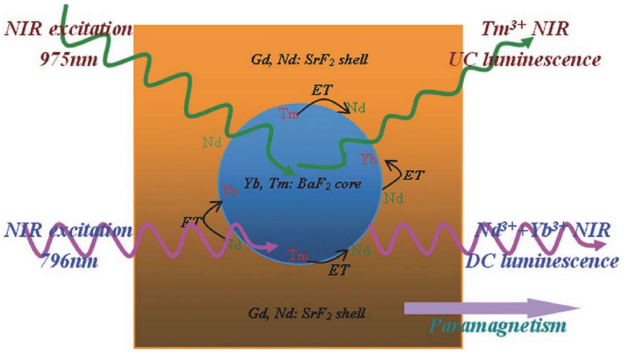

Figure 2 Schematic illustration of the energy transfer mechanisms in the Tm^{3+},Yb^{3+}:BaF_2/Gd^{3+},Nd^{3+}:SrF_2 active-core/active-shell NCs to achieve dual-modal NIR-to-NIR luminescence. Reproduced with permission.[46] Copyright 2012, Royal Society of Chemistry.

UC and Nd^{3+}, Yb^{3+} DC emissions. So core-shell structure has been adopted to design effective dual-modal NIR-to-NIR luminescence materials.

Wang *et al*.[46] have prepared ultrasmall (sub-10 nm) Tm^{3+},Yb^{3+}:BaF_2/Gd^{3+},Nd^{3+}:SrF_2 active-core/active-shell architectures. Figure 2 illustrates the energy transfer mechanisms. Tm^{3+} displayed NIR (*ca*. 800 nm) UC luminescence under 980 nm excitation through ET from Yb^{3+} to Tm^{3+}, and the Nd^{3+} ion produced NIR DC emission (*ca*. 1060 nm) upon 800 nm laser excitation. The Gd^{3+},Nd^{3+}:SrF_2 shell not only enhances NIR-to-NIR UC luminescence of the Tm^{3+}, Yb^{3+}:BaF_2 core, but also acts as the host to realize the NIR-to-NIR DC luminescence of Nd^{3+} dopants. Similarly, Qiu *et al*.[47] have constructed a β-$NaGdF_4$/Nd^{3+}@$NaGdF_4$/Tm^{3+}-Yb^{3+} core-shell nanocrystal. They utilized the typical lanthanide ions couple (namely, Tm^{3+} and Yb^{3+}) to obtain the desired NIR-to-NIR UC emission. In addition, Nd^{3+} ions were chosen as the NIR-to-NIR DC emission mode candidates for their efficient emission at around 1060 nm upon excitation at 740/800 nm. Figure 3 illustrates the fluorescence imaging of NIR-to-NIR biological tissue by the nanoparticles operating in both UC and DC modes. The above mentioned approaches provided new routes for the design of versatile nanomaterials for future luminescent bioimaging.

Enhancement of NIR-to-NIR Luminescence

Non-Ln^{3+} ions introduction

According to previous studies,[48] there are many conventional factors that can manipulate the emission intensity of Ln^{3+}-doped nanoparticles, such as dopant-host combination, particle size, phase, shape, temperature, electric-field, solvent, non-Ln^{3+} ions introduction, and metal enhancement. The enhancement of NIR-to-NIR luminescence can be realized from the above mentioned parameters. We have introduced the optimized dopant-host combinations for the NIR DC, UC and dual-modal luminescence above, thus the dopant-host combinations will not be discussed again in this part. It is well known that the emission intensities of Ln^{3+} doped NPs are partially dependent on their size and larger nanoparticles usually show stronger luminescence intensity than the smaller ones.[49] Ideally, the size of nanoparticles for biological applications should be less than 100 nm, so that the nanoparticles can be easily cleared from the body. Thus, much effort should be put forth to construct small NIR-to-NIR Ln^{3+}-doped nanoparticles with strong NIR emissions.[50] The introduction of non-Ln^{3+} ions (*e.g*. Bi^{3+}, Li^{+}, Na^{+}, Ba^{2+}, Sr^{2+} and Ca^{2+}) into to the lanthanide-doped nanoparticles is a broadly accepted strategy to gain highly bright luminescence even though the exact mechanisms for the enhancement of luminescence is still a subject of debate. In general, the main intra-4f electronic-dipole transitions

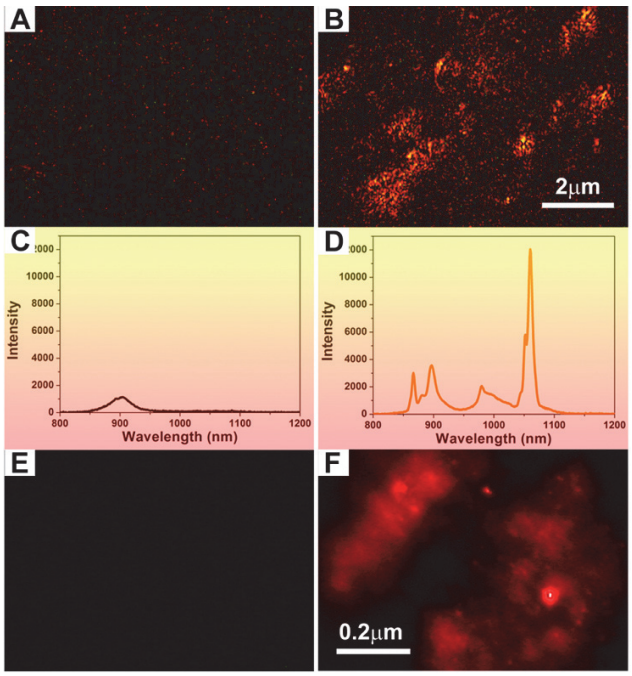

Figure 3 Fluorescence images of biological tissue before (A) and after (B) injection of dual-modal NIR-to-NIR nanoparticles under DC emission mode. (C, D) The corresponding DC luminescence spectra. Under UC emission mode, before (E) and after (F) injection of the same dual-modal NIR-to-NIR nanoparticles, luminescent images of tissue had been received. Reproduced with permission.[47] Copyright 2013, American Chemical Society.

of lanthanide ions are forbidden in consideration of the quantum mechanical selection rules. However, the tailoring of the local crystal fields is capable of breaking the forbiddance and further increasing the capability to intermix f states with higher electronic configurations, which can lead to significant increase of UCL. Song *et al.*[37] investigated NIR-to-NIR UCL in $Tm^{3+}/Yb^{3+}/Li^{+}$ triply doped Y_2O_3 nanocrystals, and they found that Li^{+} doping can greatly enhance the NIR UC emission intensity of Tm^{3+} ions. Moreover, they attributed the enhancement to the modification of the local symmetry by Li^{+}, which increased the intra-4f transitions of Tm^{3+}. In addition, the Li^{+}-doped Y_2O_3:Tm^{3+}/Yb^{3+} nanoparticles showed many other virtues, such as reducing the OH groups, dissociating the Yb^{3+} and Tm^{3+} ion clusters and creating the oxygen vacancies, which may be the other reasons for enhancement of the UCL intensities. Even though such encouraging achievements have been achieved, more methods should be explored to improve the quantum yields of NIR-to-NIR emissions in small nanocrystals.

Design of core-shell structured nanocrystals

Inspired by the size-dependent luminescence effect, enormous core-shell structures have been developed for the enhancement of NIR luminescence. A shell with similar lattice constants to the luminescent core can not only increase the size but also reduce surface quenching effect (due to large-energy vibrations of solvents and surface-associated ligands). In recent years, the core-shell structure is becoming more and more popular since the successful introduction of thermal decomposition method for shell coating in the synthesis of Ln^{3+} doped NCs in 2005.[51] Commonly, the core-shell structures can be classified into two types. For type I, an undoped inert shell is grown on the surface of a Ln^{3+}-doped active core. The luminescence efficiency of the active core/inert shell emission would increase by suppressing the nonradiative decay (due to surface defects) and quenching effect. For instance, the $KGdF_4$:Tm^{3+}, Yb^{3+} active core was coated with an inert shell of $KGdF_4$ to enhance the NIR luminescence in 2011.[36] It is assumed that the crystal defects for the core-only $KGdF_4$ nanoparticles were more than that of $KGdF_4$:Tm^{3+}2%,Yb^{3+}20%/$KGdF_4$ core-shell nanoparticles, as illustrated in Figure 4. Prasad and co-workers also proved that upon coating with a $NaYF_4$ inert shell (*ca.* 2 nm) on the $NaYbF_4$:Gd^{3+}30%/Tm^{3+}0.5% hexagonal core (*ca.* 22 nm), a dramatic 350 folds enhancement for the NIR up-conversion efficiency was achieved.[52] They also found that when $NaYbF_4$:Tm^{3+}were coated with $NaGdF_4$ shell, the emission intensity is increased by about 3 times.[53] The same group further demonstrated that high quantum yield could be achieved by suppressing nonradiative recombination originated from surface states and cross relaxations between dopants in the $NaGdF_4$:Nd^{3+}/$NaGdF_4$ NCs.[54] Besides, due to the optical transparency, stability, and small lattice mismatching with $NaYF_4$, CaF_2 has attracted more and more concern as a shell material for luminescence doped nanoparticles. Moreover, being an endogenous component in live systems, CaF_2 is likely to prevent ion leakage and be more biocompatible than the widely employed $NaYF_4$ shell. Han *et al.* have developed CaF_2 coated UCNPs that exhibit highly efficient NIR-to-NIR up-conversion luminescence.[55,56] The emission of a CaF_2 coated α-$NaYbF_4$:Tm^{3+} at 800 nm can be easily observed even in a $>$3.2 cm thick animal tissue.[57] For type II, active-core@active-shell architectures were also proposed. Except for improving NIR luminescence intensity, they are good ways to realize NIR emission with ideal excitation wavelength. For example, Zhang and co-workers[44] have fabricated a novel *β*-$NaGdF_4$/Na(Gd, Yb)F_4:Er/$NaYF_4$:Yb/$NaNdF_4$:Yb core/shell1/shell2/shell3(C/S1/S2/S3) multi-shell nano crystals as an efficient 800 to 1525 nm NIR probe for *in vivo* bioimaging. The energy transfer mechanisms are shown in Figure 5. In this NCs, 800 nm incident light was absorbed by Nd^{3+}($^4I_{9/2}\rightarrow{}^4F_{5/2}$), and then energy transference occurred between the S3 shell and the inner layer S2 ($Nd^{3+}\rightarrow Yb^{3+}$, $^2F_{7/2}\rightarrow{}^2F_{5/2}$). The energy is further transferred within the inner layers through the co-doped Yb^{3+} until the Er^{3+} in the S1 shell is sensitized ($Yb^{3+}\rightarrow Er^{3+}$, $^4I_{15/2}\rightarrow{}^4I_{11/2}$). This leads to relaxation of the excited state of Er^{3+}through releasing a 1525 nm ($^4I_{13/2}\rightarrow{}^4I_{15/2}$) photon along with phonon vibration.

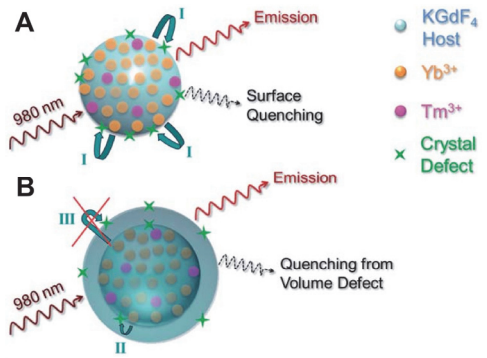

Figure 4 Schematic diagram of crystal defects for the core-only $KGdF_4$ nanoparticles (A) and $KGdF_4$:Tm^{3+} 2%, Yb^{3+} 20%/$KGdF_4$ core-shell nanoparticles (B). Reproduced with permission.[36] Copyright 2011, Royal Society of Chemistry.

In this section, we have summarized a variety of synthetic approaches for the enhancement of NIR-to-NIR emission such as introduction of non-Ln^{3+} ions and design of core-shell structured nanocrystals. We also provided examples of various systems. While there were still various aspects which could be explored to enhance NIR luminescence intensity such as phase, shape, temperature, electric-field, solvent, and metal enhancement.

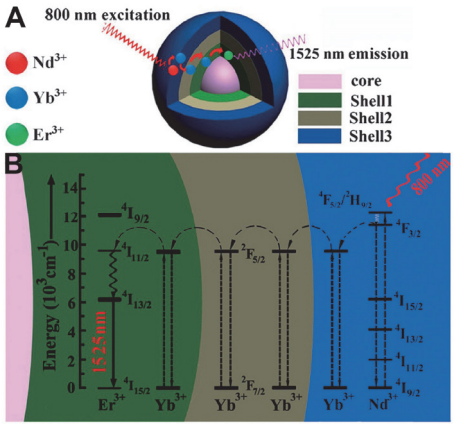

Figure 5 (A) Schematic illustration of the structure of C/S1/S2/S3 NCs. (B) Schematic representation of the energy transfer mechanisms in the multi-layer core/shell NCs. Reproduced with permission.[44] Copyright 2014, Wiley-VCH Verlag GmbH & Co. KGaA, Weinheim.

NIR-to-NIR Bioimaging Applications

As we mentioned above, NIR-to-NIR-luminescence possesses high penetration depth in biological tissues and negligible photodamage to living organisms. Therefore, NIR-to-NIR luminescent nanoparticles are ideal bioimaging agents for tracing of tumor and monitoring of therapy processes in all sorts of molecular imaging techniques. In this section, we are going to introduce the applications of NIR-to-NIR luminescent NPs for bioimaging. Specifically, the instrumentation, single mode NIR bioimaging and multimodal NIR-to-NIR bioimaging will be presented.

Instrumentation

An NIR imaging system consists of a NIR excitation laser and a NIR CCD (charge-coupled device) sensitive to wavelengths between 800 and 2000 nm. Because of the limited commercialized NIR-to-NIR imaging techniques, most groups have home designed imaging systems. Figure 6 presents a typical experimental setup for NIR-to-NIR bioimaging designed by Li's group.[31] They used two external 0—5 W adjustable 980 nm lasers to excite the sample area through coupling with fiber optics. Beam expanders were utilized to achieve a consistent excitation power density across the sampling stage and an Andor DU897 EMCCD (electron multiplying charge coupled device) was used as the detector.

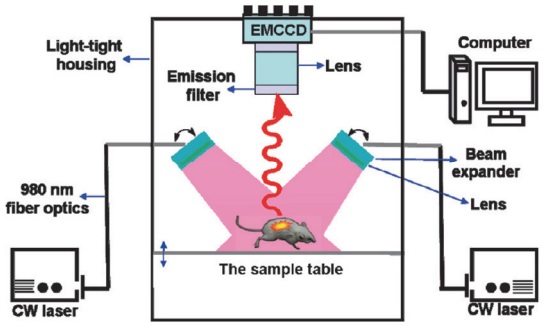

Figure 6 Diagram of the experimental setup for NIR-to-NIR *in vivo* imaging system designed by Li's group. Reproduced with permission.[31] Copyright 2009, American Chemical Society.

Silicon is the most commonly used material in CCD cameras. Standard silicon based CCD cameras are convenient for imaging of ultrafast IR laser pulses in the wavelength range 3—11 μm. But the silicon is not applicable at wavelengths longer than 1000 nm due to its low sensitivity at this region. To obtain more complementary imaging in the NIR II window, InGaAs and HgCdTe, as semiconductor alloys with narrower bandgaps, are used for near-infrared CCD cameras. From Figure 7, we can see that InGaAs cameras have a high quantum efficiency in the second near-infrared window. HgCdTe cameras suffer from lower overall quantum efficiency but were the most sensitive at longer wavelengths, which can be available in higher-resolution arrays. In general, these types of instruments provide adequate sensitivity and resolution (0.1—0.3 megapixels) for most *in vivo* imaging applications. Dai *et al.* reported *in vivo* real-time imaging of mouse hind limb vasculature in the NIR region. Biocompatible SWNT-IRDye-800 conjugates were created as dual-window imaging agents and injected to a mouse. The mouse was irradiated by a 785 nm laser at 8 $mW•cm^{-2}$ and imaged using a silicon-based CCD camera in NIR I window and an InGaAs camera equipped with different emission filters in NIR II window.[58]

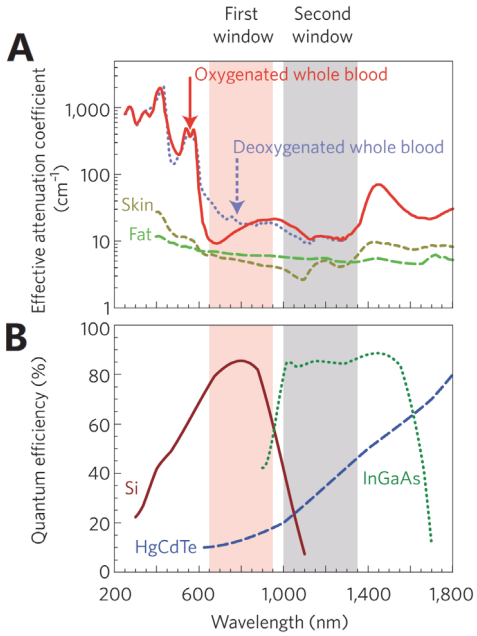

Figure 7 Optical transmission window in biological tissues. (A) Effective attenuation coefficient of oxygenated blood, deoxygenated blood, skin and fatty tissue towards light at different wavelength. (B) Sensitivity curves for typical cameras based on silicon (Si), InGaAs, and HgCdTe. Reproduced with permission.[5] Copyright 2009, Macmillan Publishers Limited.

Single Mode NIR-to-NIR Bioimaging

NIR-to-NIR bioimaging

Compared with NIR-to-vis UCL, NIR-to-NIR UCL shows higher penetration depth and makes high-contrast photoluminescence imaging possible in cells or small animals. One of the first reports on NIR-to-NIR bioimaging that utilized UC transition in Tm^{3+} and Yb^{3+} co-doped NCs demonstrated the high contrast of NIR imaging *in vivo*.[59] For most Ln^{3+}-doped UC photoluminescent nanoprobes, 980 nm laser is always used to achieve NIR-to-NIR luminescence with emission centered at around 800 nm. As we mentioned above, 980 nm light suffers from strong water absorption, tissues scattering and serious heat generation. In recent years, the excellent NIR-to-NIR PL from Nd^{3+}-doped NPs centered at 800 nm is commonly utilized in bioimaging. For instance, Zhao and co-workers have prepared Nd^{3+}-doped UC and DC dual-mode NCs for efficient *in-vitro* and *in vivo* bioimaging under excitation at 800 nm. Deep tissue penetration of the incident light, high efficiency of the DC luminescence and the *in vivo* high contrast DC imaging of the whole body of nude mouse was demonstrated. A low-power, incoherent light source can also be used as the exciting source for high-contrast NIR-to-NIR imaging. For instance, $NaGdF_4$:Nd^{3+}/$NaGdF_4$ nanoparticles with excitation at wavelength of 740 nm and PL emission at around 850—900 nm were reported. *In vivo* whole-body imaging of small animals has been successfully realized based on these NIR-to-NIR DC NCs.[54] It is worthy to mention that both excitation and the emission of these $NaGdF_4$:Nd^{3+}/$NaGdF_4$ nanoparticles are in the optical transmission window. In addition, the nanoparticles displayed high quantum efficiency, spectral sharpness, and excellent photostability. All of the above factors make these nanocrystals promising as luminescent biomaging agents.

Tumor targeting and NIR imaging

Cancer-specific NIR-to-NIR imaging shows great potential for potential application in cancer tracing in living subjects. Tumor targeting contributes to the improvement of bioimaging and treatment efficacy. Assisted with this technique, automatic accumulation of imaging and therapy agents will take place in the diseased area to reduce the collateral damage to surrounding healthy tissues, which is very important for selective kill of cancer cells in cancer therapy. Additionally, the modification of biomlecules on the surface of imaging agent provides high targeting efficiency and low toxicity. In recent years, biomolecule couples of targeting agents and receptors are important for specific recognition and gained extensive research interest, such as aptamer-corresponding substrate, antibody-antigen and FA(folic acid)-FR (folate receptor). Li *et al.* have developed an *in vivo* NIR-to-NIR targeted imaging system with high contrast and good selectivity based on RGD (arginine-glycine-aspartic peptide)-labeled UCNPs. The targeted imaging of tumors is based on the high affinity of the arginine-glycine-aspartic peptide c(RGDFK) to the $\alpha_v\beta_3$ integrin receptor that are overexpressed on the surface of tumor cells.[31] Maeda *et al.* described the application of lanthanide doped nanoparticles for tumor targeted NIR-to-NIR imaging of cancer cells and human colon cancer tissues using Er^{3+} and Yb^{3+} co-doped yttrium oxide nanoparticles functionalized with streptavidin. With biotinylated anti-EpCAM antibody on both cancer cells and human cancer tissues, cancer specific NIR-to-NIR imaging was achieved, supporting the possible application in cancer imaging.[60]

Multimodal NIR-to-NIR bioimaging

Although NIR luminescent bioimaging possesses numerous superior features, the single mode NIR-to-NIR imaging cannot meet the higher diagnosis requirement. In the last ten years several other techniques have become powerful tools in biomedical research and clinical diagnostics such as magnetic resonance imaging (MRI), X-ray computed tomography (CT). In order to gain more complementary and accurate information about the anatomical structure and physiological function, the integration of NIR-to-NIR imaging with other imaging techniques to form multimodal bioimaging is highly desired to satisfy the medical research and diagnosis requirements. Lanthanide-doped nanoparticles with NIR-to-NIR luminescence can be endowed with more promising functions to act as multimodal contrast agent and achieve multimodal bioimaging, such as

NIR-to-NIR luminescence/MRI imaging, NIR-to-NIR luminescence/CT imaging and NIR-to-NIR luminescence/MRI/CT imaging. In the following section, we will introduce some typical examples about the multimodal bioimaging applications based on lanthanide-doped nanoparticles.

NIR-to-NIR luminescence/MRI imaging

MRI is a widely used diagnostic technique based on nuclear magnetic resonance together with the relaxation of proton spins in a magnetic field.[61] MRI and NIR-to-NIR luminescence imaging are two complementary modalities that will show the advantages of both when integrated in one system, such as high spatial resolution, good sensitivity and deep tissue penetration when integrated in one system. Paramagnetic Gd^{3+} ions exhibit bright T_1-weighted MRI contrast properties owing to the existence of seven unpaired 4f electrons. What's more, Gd^{3+} ions are also widely used as the sensitizer to activate the neighboring Ln^{3+} emitters (Ln^{3+}, Er^{3+}, Ho^{3+}, Tm^{3+} and Nd^{3+}). The integration of NIR-to-NIR imaging and MRI has been achieved via Gd^{3+} doping in nanoparticles. Additionally, the Gd^{3+}-doped NCs overcome the leaching of Gd^{3+} ions in traditional Gd^{3+} chelates based MRI contrast agents. Many Gd^{3+}-doped NIR-to-NIR NPs with intense NIR emissions and tunable relaxivities ($0.14-2.27\ s^{-1}\ mM^{-1}$) have been used as NIR-to-NIR luminescent/MRI imaging contrast agents, such as $NaYbF_4$:Tm^{3+}/$NaGdF_4$,[62] GdF_3:Nd^{3+}[63,64] and $NaLuF_4$: Gd^{3+}/Yb^{3+}/Tm^{3+}.[65]

A higher r_2 relaxivity allows acquisition of high-resolution T_2-weighted MR images. The integration of NIR-to-NIR luminescent and T_2-enhanced magnetic dual functions into a single entity can be achieved with some materials with high r_2 relaxivity, such as Co^{2+} or Fe_xO_y. Shen and co-workers reported that $NaYF_4$:Yb^{3+}, Tm^{3+}, Co^{2+} NPs[66] showed a high r_2 relaxivity of 1544 $mM^{-1}\bullet S^{-1}$ due to the Co^{2+} doping, which is the highest r_2 relaxivity for multi-modality imaging compared to the previous reports. *In vivo* and *in vitro* dual-modality NIR-to-NIR UCL and T_2-weighted MR imaging of small animals have been demonstrated. Combining NIR-to-NIR emission and Fe_3O_4 into one single nanoparticle was another way to develop multifunctional nanoprobes for multimodal bioimaging. Li and co-workers[67] have reported the synthesis of bifunctional magnetic up-conversion NIR-to-NIR nanophosphors that are composed of $NaYF_4$ nanocrystals as cores and magnetic Fe_xO_y as shells. The core-shell nanocrystals have been applied in dual-modality T_2-enhanced magnetic resonance and NIR-to-NIR UCL imaging of the lymphatic system in Figure 8.

NIR-to-NIR luminescence/CT imaging

X-ray computed tomography (CT) is commonly used in medical diagnostic based on the differential X-ray absorption features of diverse tissues. This methodology offers high-resolution three-dimensional (3D) structure

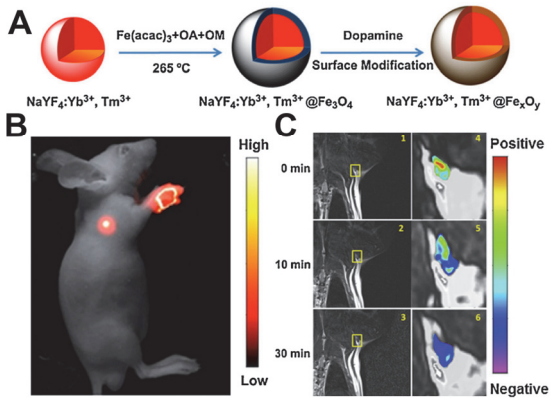

Figure 8 (A) Schematic illumination of the synthetic procedure of UCNPs@Fe_xO_y NCs. (B) *In vivo* UCL imaging of lymphatic system with UCNPs@Fe_xO_y NCs. (C) MR images of the armpit region after injection with UCNPs@Fe_xO_y NCs and color-mapped coronal images of lymph node at various time. Reproduced with permission.[67] Copyright 2014, Elsevier B.V.

details for efficient diagnostic imaging. Combining the high-resolution CT and sensitive NIR-fluorescence bioimaging could provide more accurate information for cancerous tissues in early diagnosis. Some new types of CT contrast agents, such as lanthanide ions with large atomic numbers, were developed due to their high X-ray absorption coefficient. For instance, Yb/Lu/Gd-based hosts including $NaYbF_4$, $NaLuF_4$, Yb_2O_3, $NaGdF_4$, GdF_3, Gd_2O_3 and $BaGdF_5$ NPs, have been functioning as promising CT contrast agents.[68-74] Shi and co-workers reported a simple dual-modal CT and NIR-to-NIR luminescent imaging platform based on PEGylated $NaYbF_4$:Tm^{3+} nanopaticles (NPs). The as-designed sub-20 nm nanoprobes showed excellent performances in CT and NIR-fluorescent imaging both *in vitro* and *in vivo*. Remarkably, the Yb^{3+} in the lattice of $NaYbF_4$:Tm^{3+} NPs functioned not only as a promising CT contrast medium due to its high X-ray absorption efficiency, but also as an excellent sensitizer contributing to the strong NIR-fluorescent emissions for its large NIR absorption cross-section at around 980 nm.[75]

NIR-to-NIR luminescence/MRI/CT imaging

Taking advantage of the advantages of various imaging techniques and compensating the disadvantages by constructing a multi-modal imaging system have become a fascinating strategy for generating improved quality in bioimaging. The multi-modal medical imaging has attracted great interests for providing more complementary, effective and accurate information about the physical, anatomical structure and the physiological function for diagnosis and research. The construction of NIR-to-NIR luminescence/MRI/CT trimodal imaging hold the promise to yield deep tissue penetration, high sensitivity and high spatial resolution. In the past few years, NPs containing Gd, Yb/Lu/Gd, and Er/Tm/Ho with all the imaging elements for MRI, CT and NIR-to-NIR luminescence have been developed as tri-

modal contrast agents. Li *et al.*[67] reported a multifunctional Gd^{3+} complex-modified $NaLuF_4$ nanoparticle for NIR-to-NIR up-conversion luminescence, X-ray computed tomography and T_1-enhanced magnetic resonance trimodality *in vivo* imaging. They have designed and synthesized $NaLuF_4$:Yb^{3+}, Tm^{3+}@SiO_2-GdDTPA (diethylenetriamine pentaacetic acid) and proved that the application of multi-modality *in vivo* imaging can be established successfully. The modification of Gd^{3+} complex (DTPA-Gd) on the surface of $NaLuF_4$:Yb^{3+}, Tm^{3+}@SiO_2 makes the nanoparticles positive contrast agent for T_1-weighted imaging. The observed strong X-ray absorption for CT imaging was observed due to the doped Lu^{3+} ions that possesses the largest atomic number in lanthanide.

Conclusion and Outlook

This review has summarized the recent development of NIR-to-NIR lanthanide-doped nanoparticles with emphasis on NIR luminescent properties, methods for NIR luminescence enhancement and applications in bioimaging. Their outstanding optical properties, especially deep tissue penetration and elimination of autofluorescence from biological tissues, make them ideal candidates to overcome the problems associated with traditional luminescent bioimaging agents. In addition to NIR-to-NIR luminescence, some lanthanide ions possess another attractive features such as magnetic properties and high X-ray absorption coefficient, which makes it possible to integrate several imaging techniques in a single entity to improve the quality of imaging and gain more detailed information about the biological tissues.

Despite these encouraging gains, challenges still remains in the practical bioimaging applications of NIR-to-NIR lanthanide-doped nanoparticles. One of the challenges is the low quantum yields ($<1\%$) of NIR-to-NIR luminescence due to the low absorption coefficient of lanthanide-doped nanoparticles. The low absorption coefficient is mainly limited by the low NIR absorption cross-section of Ln^{3+}, such as Yb^{3+}. Much efforts have been devoted to improve the QYs of NIR-to-NIR lanthanide-doped nanoparticles but the efforts are not very productive. Improving the QYs is still an essential task to promote the bioimaging applications of NIR-to-NIR lanthanide-doped nanoparticles. Besides, the biosafety of lanthanide-doped nanoparticles has always been a concern in bioimgaing.[76] To date, studies about the elimination of lanthanide-doped nanoparticles is limited. Several studies have reported that the elimination time for lanthanide-doped nanoparticles was weeks to months.[28,77] The elimination time determines the exposure period of lanthanide-doped nanoparticles in tissues and organs, such as the liver, lung and kidney. Generally, small size is essential for elimination. It was reported that small particles excreted by the renal route showed fast excretion. When lanthanide-doped nanoparticles were utilized as a multimodal NIR imaging probe such as an NIR-to-NIR/MRI and NIR-to-NIR/CT probe, it is highly desired that the nanoparticle size is reduced as much as possible to achieve complete elimination and a low toxicity risk. However, due to the lattice imperfections, too small size (such as less than 5 nm) inevitably leads to weak luminescence intensity. What's more, renal excretion may be difficult to carry out for this small size. For large nanoparticles, the excretion takes a long time from weeks to months and even years. In a word, the elimination is a potential limitation for bioimgaing application of lanthanide-doped nanoparticles. Besides QY and elimination, the scattering of the NIR emission also constitutes sort of concern in the bioimaging application of lanthanide-doped nanoparticles. It was reported that the penetration depth of light in NIR I window is limited to some extent due to the scattering effect caused by biological tissues.[78] However, emissions in NIR II window possess up to a 1000-fold reduction in scattering losses.[8] Considering that most of the currently reported NIR-to-NIR emissions are restricted to NIR I window, it is highly important to design novel NIR-to-NIR luminescent materials with emissions in the NIR II window. Additionally, more attention should also be paid to optimize the targeting capabilities of imaging probes and investigate the interactions of the nanoparticles with biological tissues.

The NIR-to-NIR lanthanide-doped nanoparticles have already been applied in the luminescent imaging of biological tissues and small animals. It is reasonable to expect their clinical usage in the near future in consideration of their deep tissues penetration, no autofluorescence interference and easy integration with other bioimaging techniques. In addition, the cost of the NIR-to-NIR bioimaging is quite low and can be easily made portable. All of these features suggest that the NIR-to-NIR bioimaging technique based on lanthanide-doped nanoparticles is capable of playing a critical role in biomedical science in the next few decades and further developments in QYs improvement, rapid clearance, molecular recognition optimization and imaging techniques integration will undoubtedly further strength the capabilities of current NIR-to-NIR lanthanide-doped nanoparticles.

Acknowledgement

This work was supported by the National Natural Science Foundation of China (Nos. 21201133, 21422105).

References

[1] Hong, G.; Robinson, J. T.; Zhang, Y.; Diao, S.; Antaris, A. L.; Wang, Q.; Dai, H. *Angew. Chem., Int. Ed.* **2012**, *51*, 9818.
[2] Shen, J.; Chen, G.; Vu, A.; Fan, W.; Bilsel, O.; Chang, C.; Han, G. *Adv. Optical Mater.* **2013**, *1*, 644.
[3] Weissleder, R. *Nat. Biotechnol.* **2001**, *19*, 316.
[4] Frangioni, J. V. *Curr. Opin. Chem. Biol.* **2003**, *7*, 626.
[5] Smith, A. M.; Mancini, M. C.; Nie, S. *Nat. Nanotechnol.* **2009**, *4*, 710.

[6] Weissleder, R.; Tung, C. H.; Mahmood, U.; Bogdanov, A. *Nat. Biotechnol.* **1999**, *17*, 375.
[7] Gao, X.; Cui, Y.; Levenson, R. M.; Chung, L. W. K.; Nie, S. M. *Nat. Biotechnol.* **2004**, *22*, 969.
[8] Lim, Y. T.; Kim, S.; Nakayama, A.; Stott, N. E.; Bawendi, M. G.; Frangioni, J. V. *Mol. Imaging* **2003**, *2*, 50.
[9] Hilderbrand, S. A.; Weissleder, R. *Curr. Opin. Chem. Biol.* **2010**, *14*, 71.
[10] Zhang, J.; Qiao, Z.; Yang, P.; Pan, J.; Wang, L.; Wang, H. *Chin. J. Chem.* **2015**, *33*, 35.
[11] Guo, Z. Q.; Zhu, W. H.; Zhu, M. M.; Wu, X. M.; Tian, H. *Chem. Eur. J.* **2010**, *16*, 14424.
[12] Du, Y. P.; Xu, B.; Fu, T.; Cai, M.; Li, F.; Zhang, Y.; Wang, Q.-B. *J. Am. Chem. Soc*. **2010**, *132*, 147.
[13] Chang, G.; Li, M. *Acta Chim. Sinica* **2014**, *71*, 215.
[14] Zhang, Q.; Kong, X.; Wang, X.; Cheng, C. *Chem. J. Chin. Univ.* **2014**, *35*, 224.
[15] Chen, H.-Q.; Xu, J.; Yuan, F.; Wu, Y.; Zhang, Y.-Y.; Wang, L. *Chin. Chem. Lett.* **2013**, *24*, 79.
[16] Wu, D.; Descalzo, A. B.; Weik, F.; Emmerling, F.; Shen, Z.; You, X. Z.; Rurack, K. *Angew. Chem.*, *Int. Ed*. **2008**, *47*, 193.
[17] Yu, Y. H.; Descalzo, A. B.; Shen, Z.; Rohr, H.; Liu, Q.; Wang, Y. W.; Spieles, M.; Li, Y. Z.; Rurack, K.; You, X. Z. *Chem. Asian J*. **2006**, *1*, 176.
[18] Wang, J.; Wei, T.; Li, X. Y.; Zhang, B. H.; Wang, J. X.; Huang, C.; Yuan, Q. *Angew. Chem*., *Int. Ed.* **2014**, *53*, 1616.
[19] Liu, Z.; Cai, W.; He, L.; Nakayama, N.; Chen, K.; Sun, X.; Chen, X.; Dai, H. *Nat. Nanotechnol*. **2006**, *2*, 47.
[20] Liu, Z.; Davis, C.; Cai, W.; He, L.; Chen, X.; Dai, H. *Proc. Natl. Acad. Sci. U. S. A*. **2008**, *105*, 1410.
[21] Dou, Q.; Guo, H.; Ye, E. *Mater. Sci. Eng. C* **2014**, *45*, 635.
[22] Wu, X.; Chen, G.; Shen, J.; Li, Z.; Zhang, Y.; Han, G. *Bioconjugate Chem.* **2015**, *26*, 166.
[23] Zheng, W.; Huang, P.; Tu, D.; Ma, E.; Zhu, H.; Chen, X. *Chem. Soc. Rev.* **2015**, *44*, 1379.
[24] Tu, D.; Zheng, W.; Liu, Y.; Zhu, H.; Chen, X. *Coord. Chem. Rev.* **2014** , *273–274*, 13.
[25] Chan, W. C. W.; Nie, S. M. *Science* **1998**, *281*, 2016.
[26] Liu, Y.; Tu, D.; Zhu, H.; Chen, X. *Chem. Soc. Rev.* **2013**, *42*, 6924.
[27] Tropper, A. C.; Carter, J. N.; Lauder, R. D. T.; Hanna, D. C.; Davey, S. T.; Szebesta, D. *J. Opt. Soc. Am.* **1994**, *11*, 886.
[28] Xiong, L.; Yang, T.; Yang, Y.; Xu, C.; Li, F. *Biomaterials* **2010**, *31*, 7078.
[29] Zhou, J.; Sun, Y.; Du, X.; Xiong, L.; Hu, H.; Li, F. *Biomaterials* **2010**, *31*, 3287.
[30] Yang, T.; Sun, Y.; Liu, Q.; Feng, W.; Yang, P.; Li, F. *Biomaterials* **2012**, *33*, 3733.
[31] Xiong, L.; Chen, Z.; Tian, Q.; Cao, T.-Y.; Xu, C.; Li, F. *Anal. Chem*. **2009**, *81*, 8687.
[32] Dong, N. N.; Pedroni, M.; Piccinelli, F.; Conti, G.; Sbarbati, A.; Ramírez-Hernández, J. E.; Maestro, L. M.; Iglesias-de la Cruz, M. C.; Sanz-Rodriguez, F.; Juarranz, A.; Chen, F.; Vetrone, F.; Capobianco, J. A.; Solé, J. G. ; Bettinelli, M.; Jaque, D.; Speghini, A. *ACS Nano* **2011**, *5*, 8665.
[33] Chen, G.; Ohulchanskyy, T. Y.; Kumar, R.; Ågren, H.; Prasad, P. N. *ACS Nano* **2010**, *4*, 3163.
[34] Wong, H.-T.; Chan, H. L. W.; Hao, J. *Optics Express* **2010**, *18*, 6123.
[35] Luitel, H. N.; Chand, R.; Torikai, T.; Yadaa, M.; Watari, T. *RSC Adv*. **2015**, *5*, 17034.
[36] Wong, H.-T.; Vetrone, F.; Naccache, R.; Chan, H. L. W.; Hao, J.; Capobianco, J. A. *J. Mater. Chem*. **2011**, *21*, 16589.
[37] Li, D.; Wang, Y.; Zhang, X.; Dong, H.; Liu, L.; Shi, G.; Song, Y. *J. Appl. Phys.* **2012**, *112*, 094701.
[38] Zhan, Q.; Qian, J.; Liang, H.; Somesfalean, G.; Wang, D.; He, S.; Zhang, Z.; Andersson-Engels, S. *ACS Nano* **2011**, *5*, 3744.
[39] Wang, F.; Tan, W. B.; Zhang, Y.; Fan, X.; Wang, M. *Nanotechnology* **2006**, *17*, R1.
[40] Venkatachalam, N.; Yamano, T.; Hemmer, E.; Hyodo, H.; Kishimoto, H.; Soga, K. *J. Am. Ceram. Soc.* **2013**, *96*, 2759.
[41] Li, M.; Hao, Z.-H.; Peng, X.-N.; Li, J.-B.; Yu, X.-F.; Wang, Q.-Q. *Opt. Express* **2010**, *18*, 3364.
[42] Singh, S.; Smith, R. G.; Van Uiter, L. G. *Phys. Rev. B* **1974**, *10*, 2566.
[43] Xie, X.; Gao, N.; Deng, R.; Sun, Q.; Xu, Q.; Liu, X. *J. Am. Chem. Soc*. **2013**, *135*, 12608.
[44] Wang, R.; Li, X.; Zhou, L.; Zhang, F. *Angew. Chem.*, *Int. Ed.* **2014**, *53*, 12086.
[45] Wang, Y.-F.; Liu, G.-Y.; Sun, L.-D.; Xiao, J.-W.; Zhou, J.-C.; Yan, C.-H. *ACS Nano* **2013**, *7*, 7200.
[46] Chen, D.; Yu, Y.; Huang, F.; Lin, H.; Huang, P.; Yang, A.; Wang, Z.; Wang, Y. *J. Mater. Chem*. **2012**, *22*, 2632.
[47] Zhou, J.; Shirahata, N.; Sun, H.-T.; Ghosh, B.; Ogawara, M.; Teng, Y.; Zhou, S.; Chu, R. G. S.; Fujii, M.; Qiu, J. *J. Phys. Chem. Lett*. **2013**, *4*, 402.
[48] Gai, S.; Li, C.; Yang, P.; Lin, J. *Chem. Rev*. **2014**, *114*, 2343.
[49] Yang, J.; Li, C.; Cheng, Z.; Zhang, X.; Quan, Z.; Zhang, C.; Lin, J. *J. Phys. Chem. C* **2007**, *111*, 18148.
[50] Li, Z.; Zhang, Y.; Wu, X.; Huang, L.; Li, D.; Fan, W.; Han, G. *J. Am. Chem. Soc.* **2015**, *137*, 5304.
[51] Zhang, Y.-W.; Sun, X.; Si, R.; You, L.-P.; Yan, C.-H. *J. Am. Chem. Soc*. **2005**, *127*, 3260.
[52] Damasco, J. A.; Chen, G.; Shao, W.; Ågren, H.; Huang, H.; Song, W.; Lovell, J. F.; Prasad, P. N. *ACS Appl. Mater. Interfaces* **2014**, *6*, 13884.
[53] Chen, G.; Ohulchanskyy, T. Y.; Ågren, H.; Prasad, P. N. *Nanoscale* **2011**, *3*, 2003.
[54] Chen, G.; Ohulchanskyy, T. Y.; Liu, S.; Law, W.-C.; Wu, F.; Swihart, M. T.; Ågren, H.; Prasad, P. N. *ACS Nano* **2012**, *6*, 2969.
[55] Shen, J.; Chen, G.; Ohulchanskyy, T.; Kesseli, S.; Buchholz, S.; Li, Z.; Prasad, P.; Han, G. *Small* **2013**, *9*, 3213.
[56] Punjabi, A.; Wu, X.; Tokatli-Apollon, A.; El-Rifai, M.; Lee, H.; Zhang, Y.; Wang, C.; Liu, Z.; Chan, E.; Duan, C.; Han, G. *ACS Nano* **2014**, *8*, 10621.
[57] Chen, G.; Shen, J.; Ohulchanskyy, T.; Patel, N.; Kutikov, A.; Li, Z.; Song, J.; Pandey, R.; Ågren, H.; Prasad, P.; Han, G. *ACS Nano* **2012**, *6*, 8280.
[58] Hong, G.; Lee, J. C.; Robinson, J. T.; Raaz, U.; Xie, L.; Huang, N. F.; Cooke, J. P.; Dai, H. *Nat. Med*. **2012**, *18*, 1841.
[59] Nyk, M.; Kumar, R.; Ohulchanskyy, T. Y.; Bergey, E. J.; Prasad, P. N. *Nano Lett.* **2008**, *8*, 3834.
[60] Zako, T.; Yoshimoto, M.; Hyodo, H.; Kishimoto, H.; Ito, M.; Kaneko, K.; Soga, K.; Maeda, M. *Biomater. Sci*. **2015**, *3*, 59.
[61] Brown, M. A.; Semelka, R. C. *Textbook of MRI*: *Basic Principles and Applications*, Wiley-Liss, New York, **2003**, pp. 11—20.
[62] Zhang, X.; Zhao, Z.; Zhang, X.; Cordes, D. B.; Weeks, B.; Qiu, B.; Madanan, K.; Sardar, D.; Chaudhur, J. *Nano Res*. **2015**, *8*, 636.
[63] Mimun, L. C.; Ajithkumar, G.; Pokhrel, M.; Yust, B. G.; Elliott, Z. G.; Pedraza, F.; Dhanale, A.; Tang, L.; Lin, A.-L.; Dravidd, V. P.; Sardar, D. K. *J. Mater. Chem. B* **2013**, *1*, 5702.
[64] Pokhrel, M.; Mimun, L. C.; Yust, B.; Kumar, G. A.; Dhanale, A.; Tang, L.; Sardar, D. K. *Nanoscale* **2014**, *6*, 1667.
[65] Zeng, S.; Xiao, J.; Yang, Q.; Hao, J. *J. Mater. Chem*. **2012**, *22*, 9870.
[66] Xia, A.; Zhang, X.; Zhang, J.; Deng, Y.; Chen, Q.; Wu, S.; Huang, X.; Shen, J. *Biomaterials* **2014**, *35*, 9167.
[67] Xia, A.; Gao, Y.; Zhou, J.; Li, C.; Yang, T.; Wu, D.; Wu, L.; Li, F. *Biomaterials* **2011**, *32*, 720.
[68] Liu, Z.; Pu, F.; Huang, S.; Yuan, Q.; Ren, J.; Qu, X. *Biomaterials* **2013**, *34*, 1712.
[69] Xing, H.; Bu, W.; Ren, Q.; Zheng, X.; Li, M.; Zhang, S.; Qu, H.; Wang, Z.; Hua, Y.; Zhao, K.; Zhou, L.; Peng, W.; Shi, J. *Biomaterials* **2012**, *33*, 5384.
[70] Cheung, E. N. M.; Alvares, R. D. A.; Oakden, W.; Chaudhary, R.; Hill, M. L.; Pichaandi, J.; Mo, G. C. H.; Yip, C.; Macdonald, P. M.;

Stanisz, G. J.; van Veggel, F. C. J. M.; Prosser, R. S. *Chem. Mater*. **2010**, *22*, 4728.
[71] Liu, Y.; Ai, K.; Liu, J.; Yuan, Q.; He, Y.; Lu, L. *Angew. Chem., Int. Ed*. **2012**, *51*, 1437.
[72] Liu, Z.; Li, Z.; Liu, J.; Gu, S.; Yuan, Q.; Ren, J.; Qu, X. *Biomaterials* **2012**, *33*, 6748.
[73] Zeng, S.; Tsang, M.-K.; Chan, C.-F.; Wong, K.-L.; Hao, J. *Biomaterials* **2012**, *33*, 9232.
[74] Xing, H.; Bu, W.; Ren, Q.; Zheng, X.; Li, M.; Zhang, S.; Qu, H.; Wang, Z.; Hua, Y.; Zhao, K.; Zhou, L.; Peng, W.; Shi, J. *Biomaterials* **2012**, *33*, 5384.
[75] Xia, A.; Chen, M.; Gao, Y.; Wu, D.; Feng, W.; Li, F. *Biomaterials* **2012**, *33*, 5394.
[76] Sun, Y.; Feng, W.; Yang, P.; Huang, C.; Li, F. *Chem. Soc. Rev.* **2015**, *44*, 1509.
[77] Liu, C.; Gao, Z.; Zeng, J.; Hou, Y.; Fang, F.; Li, Y.; Qiao, R.; Shen, L.; Lei, H.; Yang, W.; Gao, M. *ACS Nano* **2013**, *7*, 7227.
[78] Wang, R.; Zhang, F. *J. Mater. Chem. B* **2014**, *2*, 2422.

(Lu, Y.)

